Electromechanical modelling of a new class of nanocomposite cement-based sensors for structural health monitoring

Antonella D'Alessandro[*], Filippo Ubertini[*], Annibale Luigi Materazzi[*], Simon Laflamme[‡,•], Maurizio Porfiri[†]

[*]*Department of Civil and Environmental Engineering, University of Perugia, Perugia, 06125, Italy*

[‡]*Department of Civil, Construction and Environmental Engineering, Iowa State University, Ames, IA 50011, USA*

•*Department of Electrical and Computer Engineering, Iowa State University, Ames, IA 50011, USA*

[†]*Department of Mechanical and Aerospace Engineering, New York University Polytechnic School of Engineering, Brooklyn, NY 11201*

Abstract. This work focuses on the analysis of a new nanocomposite cement-based sensor (carbon nanotube cement-based sensor), for applications in vibration-based structural health monitoring of civil engineering structures. The sensor is constituted of a cement paste doped with multi walled carbon

This article is from *Structural Health Monitoring*, ***14(2), 2015: 137-147 doi: 10.1177/1475921714560071. posted with permission.***

nanotubes, so that mechanical deformations produce a measurable change of the electrical resistance. Prior work of some of the authors has addressed the fabrication process, dynamic behaviour, and implementation to full-scale structural components. Here, we investigate the effectiveness of a linear lumped-circuit electromechanical model, in which dynamic sensing is associated with a strain-dependent modulation of the internal resistance. Salient circuit parameters are identified from a series of experiments where the distance between the electrodes is parametrically varied. Experimental results indicate that the lumped-circuit model is capable of accurately predicting the step response to a voltage input and its steady-state response to a harmonic uniaxial deformation. Importantly, the model is successful in anticipating the presence of a superharmonic component in sensor's output.

Keywords: Carbon nanotubes, Electromechanical model, Nanotechnology, Smart materials, Smart sensors, Structural health monitoring

1. INTRODUCTION

Civil engineering structures are subject to materials' aging and severe loading conditions that contribute to progressive degradation and loss of safety [1]. Due to the advanced state of degradation of infrastructural systems in western countries, there is a pressing need to device tools for accurately assessing structural integrity and afford condition-based maintenance [2]. Structural Health Monitoring (SHM) is expected to contribute to this field of study by enabling automated analysis of data collected on-site by sensing systems [3]. Examples of SHM applications include aftershock rapid assessment [4], optimal scheduling of maintenance activities [5], and effective monitoring of deterioration [6], and fatigue of structural components [7].

New multifunctional and smart materials with a tremendous potential in SHM have recently emerged, owing to recent adances in the field of nanotechnology [8]. Particularly interesting are those materials that display self-sensing abilities, whereby their electrical response is modulated by their state of strain [9,10]. In this context, cement-based materials have often been used as matrices in strain-sensitive nanotechnology-modified composites [11,12]. For example, the incorporation of micro- and nano-fibers to cementitious matrices has been shown to significantly influence their chemical, physical and mechanical properties in many ways (see for example [13,14]). From an electrical perspective, cement-based materials primarily behave as dielectrics, whereby an imposed electric field induces the orientation of dipoles in the material so as to create an induced electric field opposite to the applied one. The resulting polarization is responsible for the decrease of the electric current over time under the application of a constant potential difference [15,16].

Several studies have analysed smart sensors consisting of cement-based materials doped with carbon nanoinclusions [8-24]. A particularly promising strain sensor based on a multifunctional cement-based composite material, termed Carbon NanoTube Cement-based Sensor (CNTCS), has been recently developed by some of the authors [20-22]. The sensor consists of a cement paste doped with Multi Walled Carbon Nanotubes (MWCNTs), which enable the transduction of a mechanical strain into a measurable variation of the electrical resistance. The inclusion of conductive additives to the cementitious matrix improves the composite conductivity until the percolation threshold is reached, above which the inclusions are in physical contact and form a conductive network. The electrical conductivity of such composites is remarkably affected by the electrical properties of the additives, as well as their degree of dispersion. In particular, MWCNTs tend to spontaneously agglomerate due to their small dimensions and high specific surface area, which enhances Van der Waals attraction forces [25]. The use of physical dispersants can help preventing the formation of

bundles in an aqueous solution containing Carbon NanoTubes (CNTs), yet ultrasonic treatment is necessary to achieve a satisfactory dispersion [26,27].

Based on experimental findings in [20], this sensor is expected to afford strain measurements in concrete structures with an accuracy similar to that of conventional strain gauges. In addition to measurement accuracy, the sensor offers three main benefits: i) long usable lifetime, due to its limited exposure to environmental agents; ii) high sensing performance, due to superior bonding to the structure; and iii) monitoring capability of large surfaces and volumes. While previous studies on CNTCS [21,22] have demonstrated the feasibility of dynamic strain sensing in concrete structures using CNTCSs, a tractable electromechanical model is yet to be developed.

Most of the literature on cement-based materials doped with carbon inclusions has focused on fabrication and experimental characterization, and theoretical studies explaining the physical principles underlying their complex behaviour are limited. For example, some efforts have shown that carbon fibers and nanotubes could modify the electrical resistivity of cementitious materials due to piezoresistivity associated with the slight pull-out of the fibres passing through microcracks [23,28]. Other studies have proposed models to characterize physical behaviour, which includes lumped-circuit models of carbon fibre cement paste sensors based on series-parallel arrays of electrical resistors [29-31] and capacitors [32]. In these models, the resistance of cement paste sensors is associated with the intrinsic resistance of the material, the resistance of the electrodes, and the contact resistance between electrodes and cement paste. The capacitance is instead related to electric polarization [31].

In this paper, we assess a mathematically-tractable electromechanical model for CNTCSs developed in [20], based on a lumped passive circuit similar to that proposed in [32]. The model consists of a capacitor, associated with the internal polarization of the composite, and two resistors, related to the conductivity of the

electrodes-sensors interface and the composite. The mechanical deformation of the composite modulates the circuit parameters, thus resulting into a strain-dependent electrical response of the sensor. The model is expected to provide important insights into the complex behaviour of CNTCSs, aid the development of signal processing tools for dynamic sensing using CNTCSs, and guide the selection of application-specific fabrication methods.

The rest of the paper is organized as follows. Firstly, details on the fabrication and potential applications of CNTCSs are presented; secondly, the electromechanical model is introduced and a methodology for its experimental validation is presented; and, finally, experimental results are presented and discussed.

2. CARBON NANOTUBE CEMENT-BASED SENSORS

2.1 Fabrication procedure

A prismatic specimen of CNTCS with dimension of 50×40×50 mm^3 is fabricated using cement type Portland 42.5 and Arkema MWCNTs type Graphistrength C100. Carbon content of such MWCNTs is greater than 90%. Furthermore, MWCNTs have an outer mean diameter between 10 and 15 nm and a length between 0.1 and 10 μm. The average number of walls ranges from 5 to 15. The MWCNTs used for the sample are in the amount of 2% by weight of cement. The water-cement ratio of the mixture is 0.43. Sky 521 plasticizer, based on second-generation polycarboxylate ether (PCE) polymers, is added, in the amount of 1% by weight of cement, to improve workability. No aggregate (neither fine nor coarse) is used. The mix design of the cement paste is summarized in Table 1. The table lists the components by weight for a cubic meter of cement paste and for the single specimen.

As discussed in [13,14], the process of adding MWCNTs to the cement mix is rather delicate, due to the tendency of the particles to agglomerate. To produce bundle-free homogeneous three-dimensional MWCNT

networks, the dispersion of MWCNTs is performed in two consecutive phases. In the first phase, MWCNTs are spread in deionized water mixed with addiction of ByK154 chemical dispersant. ByK154 is an acrylate copolymer ammonium salt solution (Fig. 1(a), (b)). Mixing is obtained through 10 minutes of magnetic stirrer (Fig. 1(c)), 15 minutes of sonication (Fig. 1(d)), and 15 minutes of mechanical mixing (Fig. 1(e)).

In the second phase, the water suspension and the plasticizer are added to the cement powder and manually mixed with a metallic stick (Fig. 1(f)). The material is then poured into oiled molds (Fig. 1(g)) and the electrodes are embedded in the paste (Fig. 1(h)). After settling, the sample is unmolded for curing (Fig. 1(i)). Figure 1(j) is a picture of the resulting Carbon NanoTube Cement-based Sensor.

The quality of the dispersion of MWCNTs in the matrix is ascertained through micrographs from a Scanning Electron Microscope (SEM). A few representative micrographs are shown in Fig. 2, demonstrating good dispersion of MWCNTs in the aqueous solution, Fig. 2(a), and in the cement paste, Fig. 2 (b). The embedded electrodes consist of stainless steel nets that are directly inserted in the specimens along approximately 75% of their thickness. In each specimen, four electrodes are placed symmetrically along the central axis. Specifically, the two inner electrodes are placed at a distance of 2 cm, the external electrodes have a relative distance of 4 cm, and the distance between an internal and an external electrode is 1 cm, as shown in Fig. 3.

TABLE 1. Mix design of nanocomposite cement paste

Components	**Content**	
	(kg/m^3)	**(g/sample)**
MWCNTs	33.0	3.9
Ammonium polyacrylate-based dispersant ByK154	3.3	0.4
Portland cement 42.5	1652	195
Polycarboxylate ether-based plasticizer Basf Glenium Sky 521	16.5	1.9

Water	710	84
Water/cement ratio	0.43	0.43

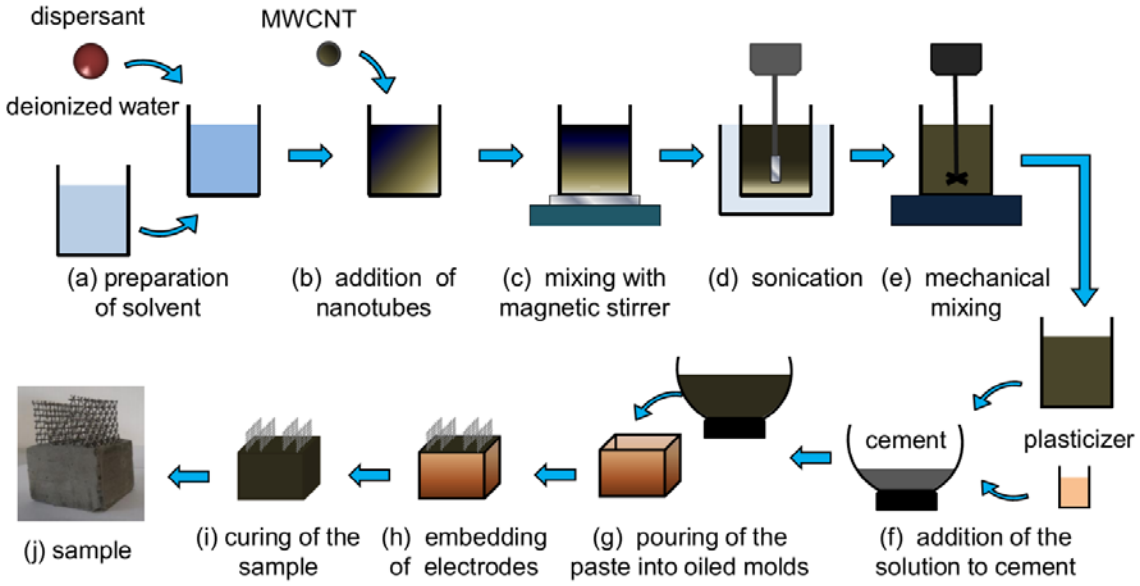

FIGURE 1. Preparation scheme of CNTCS with embedded steel net electrodes.

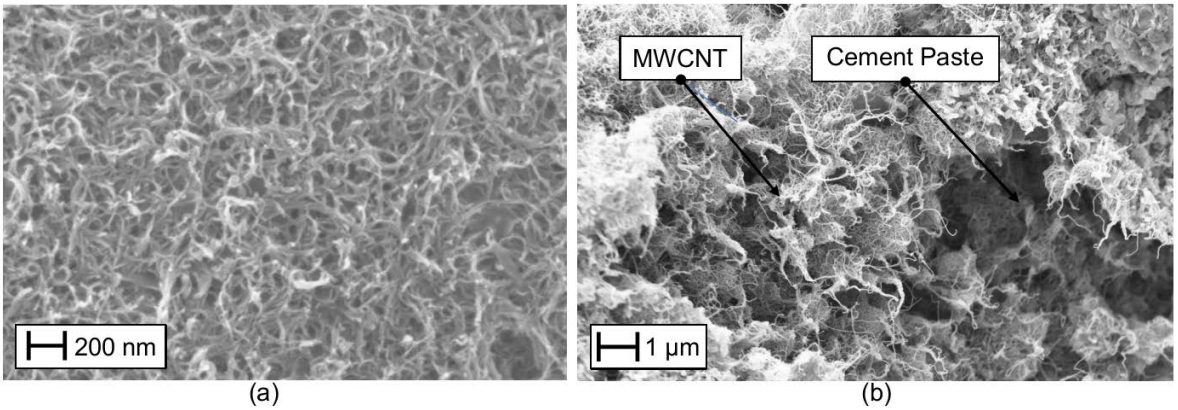

FIGURE 2. Scanning electron micrographs of water solution with MWCNT (a) cement paste with MWCNT (b).

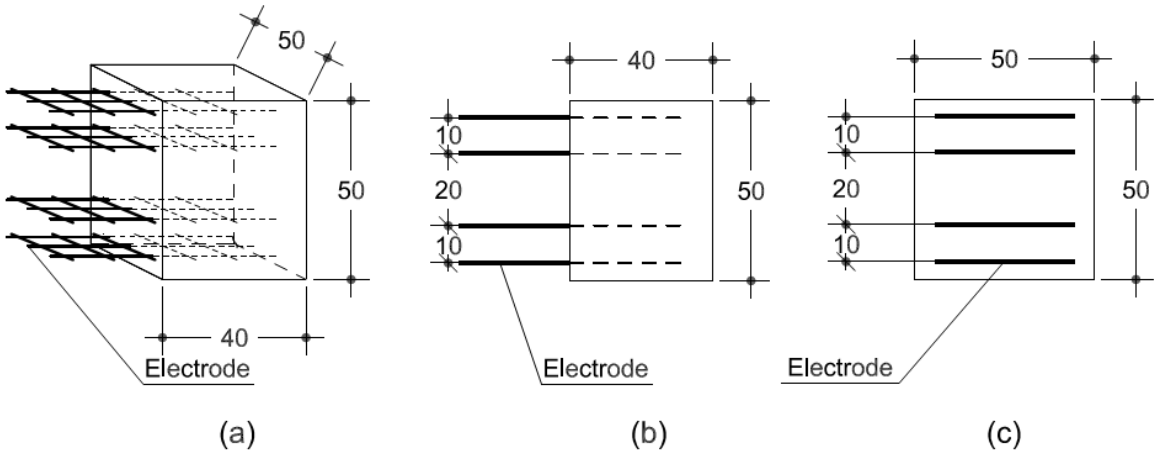

FIGURE 3. Sketch and dimensions (in mm) of the Carbon Nanotube Cement-based Sensor: axonometric view (a), side view (b), and front view (c).

2.2 Potential applications

The novel CNTCS shoud be considered as a first step toward the development of a low-cost, durable, and spatially distributed sensing system for concrete structures. Being fabricated from a material similar to structural concrete, the sensor can be embedded within the structure to afford distributed self-sensing over large volumes. Although the current design of CNTCS does not contain any aggregate, future developments may utilize concrete as matrix. Moroever, the structure itself could be entirely or partially casted from sensing concrete.

The CNTCS provides strain measurements that can be directly used for local structural health assessment and crack detection. Structural degradation could be assessed globally or at a substructural level, by measuring the strain in different locations at high sampling rates while implementing established vibration-based health assessment procedures [3]. Different from acceleration measurements, the direct measurent of the strain enables a more accurate evaluation of the displacement in time [33].

Although only few studies have addressed the long-term behaviour of cement-based sensors [34], we hypothesize that CNTCSs may outperform off-the-shelf sensors, due to the higher durability of cement-based materials. Feasible structural health monitoring applications for CNTCSs include historic masonry structures and concrete structures (e.g., buildings, bridges, dams, and pavements).

3. ELECTROMECHANICAL MODEL

Recent findings from the technical literature [31,32] suggest that the electrical behaviour of cement-based composites doped with carbon fibres and carbon nanotubes can be effectively modelled through interconnected capacitors and resistors. Based on these studies, here we assess a minimal lumped-circuit model to characterize the electromechanical behaviour of CNTCSs.

To elucidate the electrical behaviour of the CNTCS in the absence of mechanical deformations, the samples are connected to a power source providing a stabilized potential difference across their electrodes,

V , and to a digital multimeter measuring the time trace of the current passing through the specimen, $I_0(t)$, as illustrated in Figure 4 (a), where t is the time variable. In order to minimize electromagnetic interference, coaxial cables are used to connect the power source, the sensor, and the multimeter. The active volume of the specimen, defined as the portion of the sensor in between the selected pairs of electrodes, is modelled as the parallel connection of a capacitor and a resistor. The equivalent electrical circuit along with measurement hardware and the specimen is shown in the bottom part of Figure 4 (a), where R_0 and C_0 denote internal resistance and capacitance, respectively, and R_c encapsulates contact resistances for cables, electrodes, and the specimens. In this case, the time evolution of the current through the sample is governed by the following differential equation:

$$\dot{I}_0(t) + \frac{I_0(t)}{\tau} = \frac{V}{\tau \overline{R}} \tag{1}$$

where a superimposed dot denotes time differentiation, $\overline{R} = R_0 + R_c$, and

$$\tau = \frac{C_0 R_0 R_c}{\overline{R}} \tag{2}$$

is the characteristic time of the circuit. By varying the distance, d_0, between the selected electrodes the active volume varies and, consequently, R_0 and C_0 should change, while R_c should remain approximately constant.

In a second series of experiments, a compressive axial load, N, induces a mechanical deformation of the sensor and, consequently, a small variation of the distance between the active electrodes, Δd, shown in Fig. 4. This variation is, in turn, expected to modulate the time evolution of the electrical properties of the CNTCS with respect to the nominal values. On the basis of findings in [32], we hypothesize that only the internal resistance is influenced by the mechanical deformation, so that the resistance changes as $R = R_0 + \Delta R$, where

ΔR is the incremental change. In addition, the relationship between the relative change in the internal electrical resistance, $\Delta R/R_0$, and the axial strain, ε (positive in compression) is assumed to be linear, that is,

$$\frac{\Delta R}{R_0} = -\lambda\varepsilon \tag{3}$$

where λ represents the gauge factor of the sensor.

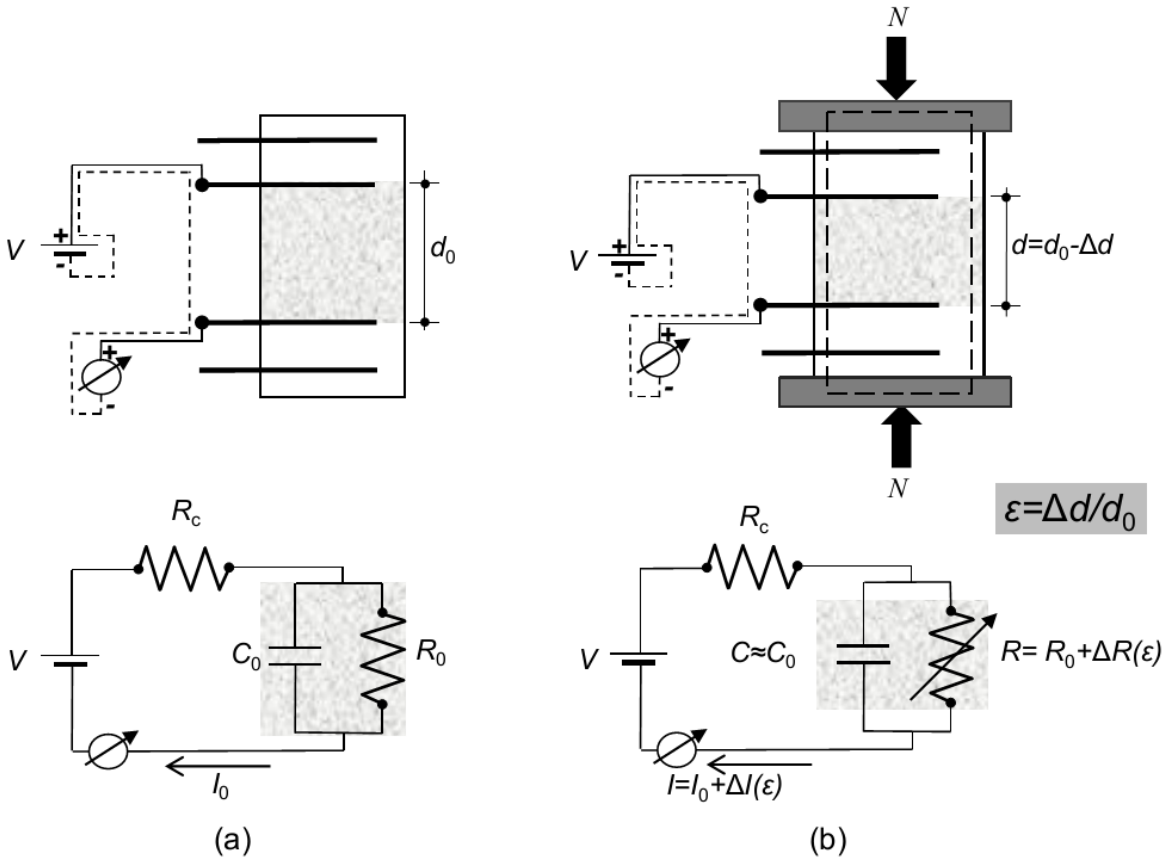

FIGURE 4. Schematic of the proposed electromechanical model of a CNTCS: unloaded (a) and loaded samples (b).

As illustrated in Figure 4 (b), the current through the sensor, $I(t)$, under the stabilized voltage, V, and time-varying axial strain, $\varepsilon(t)$, is measured using a multimeter to elucidate the possibility of dynamic sensing. From the proposed model, the time evolution of current is governed by the following ordinary differential equation with time-varying coefficients, which can be directly obtained from the analysis of the electrical circuit in Figure 4 (b):

$$\dot{I}(t)+\frac{1}{\tau\overline{R}}\left(R_0+\frac{R_c}{1-\lambda\varepsilon}\right)I(t)=\frac{1}{1-\lambda\varepsilon}\frac{V}{\tau\overline{R}} \tag{4}$$

4. EXPERIMENTAL METHODS

4.1 Experimental setup

A series of experiments are conducted to verify the equivalent circuit model adopted for CNTCSs. The electrical behaviour of the CNTCS is studied in a first study, and the strain sensing capabilities is investigated in a second study. The experimental setup is illustrated in Fig. 5. National Instruments NI PXIe-1073 chassis is used to acquire data. A source measure unit, model NI PXI-4130, generates the stabilized potential difference V that is applied to the electrodes of the specimens through coaxial cables. The electrical current through the sample is measured using a high speed digital multimeter, model NI PXI-4071.

Dynamic characterization is conducted using a servo-controlled pneumatic universal testing machine (IPC Global UTM-14P) with 14 kN load capacity, equipped with an environmental chamber to control for constant temperature. The specimen is subjected to harmonic loading of fixed frequency and varying magnitude, and the electrical response is simultaneously studied following the same approach described above. The applied axial deformation is measured through two off-the-shelf resistive strain gauges attached on opposite lateral

faces of the specimen, whose outputs are recorded via a data acquisition bridge input module, model NI PXIe-4330.

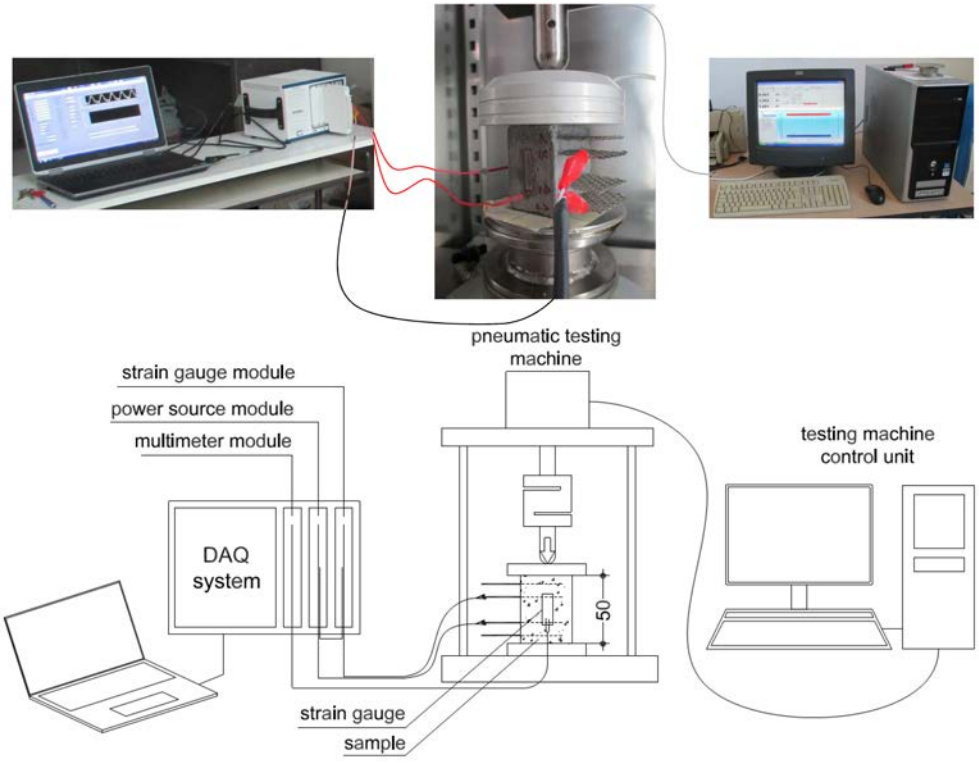

FIGURE 5. Experimental setup. From left to right, data acquisition system, sample placed in the axial pneumatic testing machine, and testing machine control unit.

4.2 Test Series 1: Unloaded specimen

The objective of the first series of tests is to verify the validity of the lumped electrical circuit model in the absence of mechanical deformations. The time trace of the electrical current, $I_0(t)$, in response to a constant

voltage difference, $V = 1.5$ V, is measured for different electrode distances. For consistency, all the measurements are performed with a common electrode, so that the following distances are investigated: d_0 = 1, 3, and 4 cm.

Integrating Eq. (1) as a function of time with initial condition $I_0(0) = V/R_c$ yields

$$I_0(t) = \frac{V}{\overline{R}}\left(\frac{R_0}{R_c}\exp\left(-\frac{t}{\tau}\right)+1\right) \tag{5}$$

For each configuration of active electrodes, the electrical parameters R_c, R_0, and C_0 are estimated by curve-fitting the measured response using Eq. (5). In particular, R_c is directly obtained from the initial value of measured current intensity, while R_0 and C_0 are found from non linear least square fitting. For each value of d_0, the current output is measured for a total duration of 1 hr and sampled at 1 kHz. The accuracy of the model is verified by the quality of fitting and the consistency of R_c.

4.3 Test Series 2: Loaded specimen

The objective of the second series of tests is to assess the possibility of predicting strain sensing using the investigated circuit model. Tests are performed for varying distances between electrodes (d_0 = 1, 3, and 4 cm) and for varying amplitudes of the applied harmonic axial load at 5 Hz. The applied sinusoidal loads have a mean value of 1 kN and amplitudes of 0.3, 0.4, 0.5, and 0.6 kN. Given the cross-sectional area of 2000 mm^2, the amplitude of the pulsating compressive stress, σ, varies from 0.15 to 0.3 MPa. The response of the sensors is measured for a total duration of 600 s under application of a constant voltage difference $V = 1.5$ V and sampled at 1 kHz. Considering each test permutation (electrode distance and loading amplitude) yields a total of 16 tests.

The model posits that the response of the sensor to a harmonic axial deformation of amplitude E and circular frequency ω is governed by the following linear differential equation with time-varying coefficients:

$$\dot{I}(t)+\frac{1}{\tau\overline{R}}\left(R_0+\frac{R_c}{1-\lambda E\sin(\omega t)}\right)I(t)=\frac{1}{1-\lambda E\sin(\omega t)}\frac{V}{\tau\overline{R}} \tag{6}$$

where the effect of the mechanical pre-stress on the mean internal resistance is discarded. The solution of Eq. (6) can be written in closed-form following [36]. However, assuming that the time period of the mechanical loading is sufficiently smaller than the internal characteristic time of the circuit, namely $2\pi/\omega << \tau$, the apparent electrical resistance, $R_a(t)$, defined as the ratio between the imposed voltage and the measured current can be approximated as [36]

$$R_a(t)=\frac{V}{I(t)}\cong R_a^0(t)+R_a^t(t) \tag{7}$$

where $R_a^0(t)$ is a slowly varying component related to charge build-up in the capacitor and $R_a^t(t)$ is a fast component associated to strain sensing. This latter quantity is generally written as

$$R_a^t(t)=-R_0\lambda E\sum_{n=1}^{\infty}a_n\sin(n\omega t+\phi_n) \tag{8}$$

Here, a_n and ϕ_n are a set of coefficients and phase lags depending on ω and on τ which can be determined from the solution of Eq. (6). Thus, Eq. (8) describes a harmonic distortion with respect to the monochromatic input, thus suggesting that the response of the sensor is characterized by superharmonic components generated by the sinusoidal axial strain. This phenomenon is not related to nonlinearities, but only to the time-varying nature of the governing linear differential equation [36]. The case of an ideal

transducer corresponds to $a_1 = 1$ and $a_2 = a_3 = ... = a_\infty = 0$, and is obtained when the characteristic time of the circuit becomes infinite.

In the experiments, the slowly varying component, $R_a^0(t)$, in Eq. (7) is eliminated from the measured response by subtraction of a high order (20th order) polynomial fitting of the time trace of $R_a(t)$. Then, the amplitudes of the harmonics in Eq. (8) are obtained by Fast Fourier Transform (FFT) analysis. In particular, multiple windowing of the signal is implemented and the FFT is computed for each time window containing $n_t = 2^{15}$ samples. The amplitude of the generic harmonic at a frequency $n\omega$ is obtained by multiplying the absolute value of the FFT corresponding to that frequency by $2/n_t$. Finally, averages of the different windows are aggregated to calculate the average amplitudes of the harmonics.

The amplitude of the first harmonic of the apparent resistance in Eq. (8) is used for estimating the gauge factor, λ. Therein, *E* is taken as the amplitude of the time-varying average strain measured by the two strain gauges, while the mean internal resistance, R_0, is assumed to be unaffected by the presence of the mechanical loading. Linearity of the sensor is assessed by verifying that λ does not vary with the strain amplitude *E*. On the other hand, λ is expected to change as a function of the distance between the active electrodes due to the change of the active sensor volume.

5. EXPERIMENTAL RESULTS

5.1 Step response of the unloaded specimen

Step responses of the specimen in absence of mechanical deformations are presented in Figure 6. Comparison between experimental findings and model predictions support the feasibility of utilizing the proposed circuit model to elucidate the electrical response of the sensor.

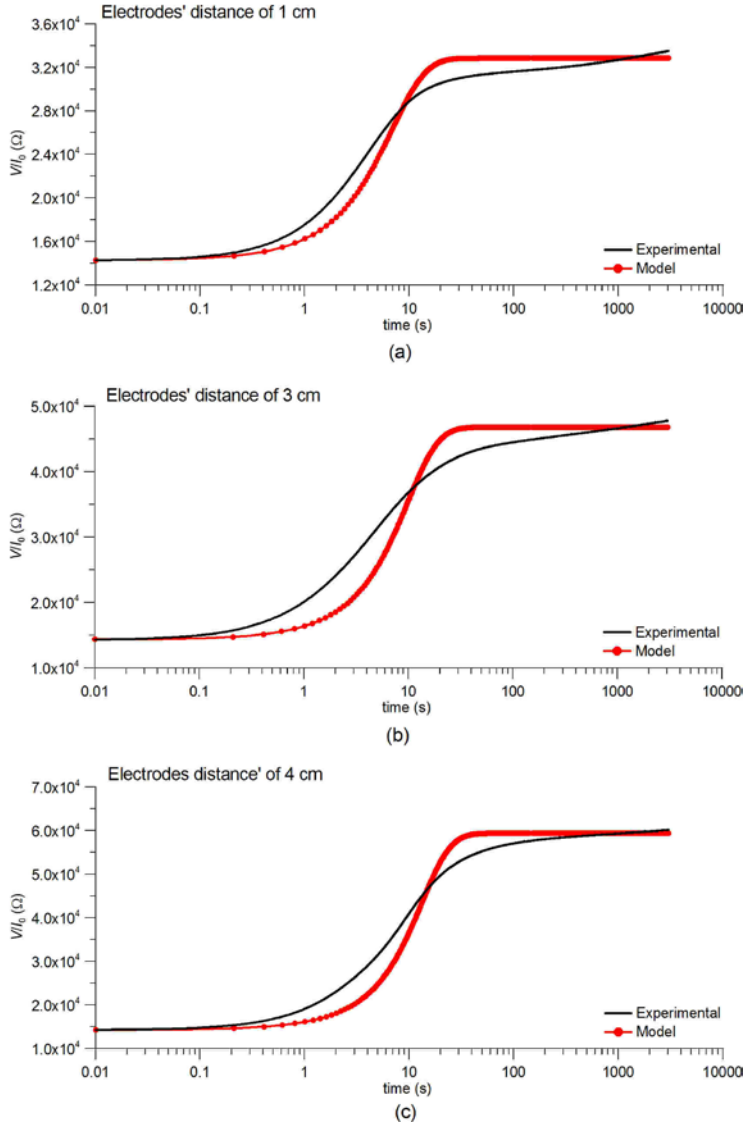

FIGURE 6. Comparison between experimental results and analytical predictions for the step response of CNTCSs with varying distances between the active electrodes: 1 cm (a); 3 cm (b); and 4 cm (c).

Distance between electrodes

	1 cm	3 cm	4 cm
R_c (kΩ)	14.29	14.34	14.32
R_0 (kΩ)	18.55	32.47	45.09
C_0 (μF)	515	510	567
τ (s)	4.16	5.07	6.16

TABLE 2. Model parameters from electrical step responses for the specimen with varying distance between active electrodes.

Fitting the step responses using Eq. (5) allows for the identification of salient parameters of the electrical circuit, R_c, R_0, and C_0, for each configuration of active electrodes. The results, summarized in Table 2, confirm that contact resistance does not vary when the distance between active electrodes is changed. On the other hand, the internal resistance increases with d_0 due to changes in the active volume of the sensor and increasing length of the electrical paths developing inside the specimen. While the internal resistance exhibits prominent variations as it is more than doubled as the distance between the electrodes is increased from 1 to 4 cm, the variations of the capacitance appear to be secondary. Perhaps, the capacitance is influenced by double layer or other local charge accumulation phenomena [37], which do not scale with the physical distance between the electrodes.

5.2 Steady-state response of loaded specimens

Figure 7 reports the time trace of the apparent electrical resistance, that is, the ratio between the input voltage and the output current (a) along with its power spectral density (PSD) (b) obtained under the 5Hz harmonic loading. In agreement with Eq. (8), results reported therein demonstrate that the dynamic response

of the sensor is not monochromatic, but rather contains superharmonics at 10 Hz, 15 Hz, and other multiples of 5Hz. Notably, results in Table 2 also confirm that the characteristic time scale of the electrical response is considerably slower than the period of mechanical loading.

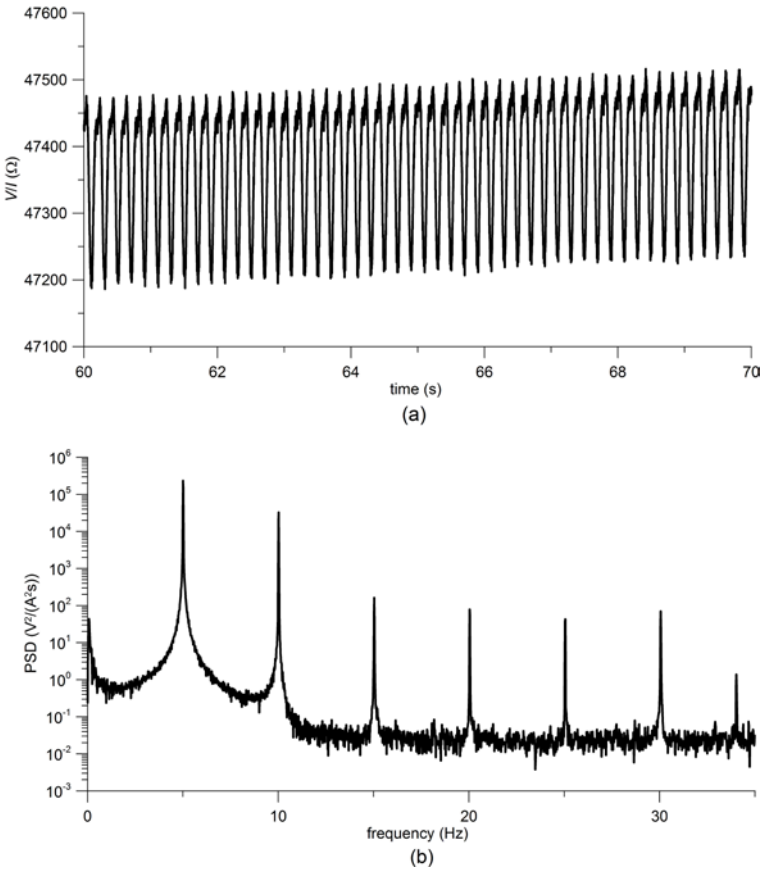

FIGURE 7. Variation of apparent resistance (a) and its PSD (b) under 5 Hz sinusoidal axial loading (1±0.5 kN) for a distance between the electrodes of 3 cm.

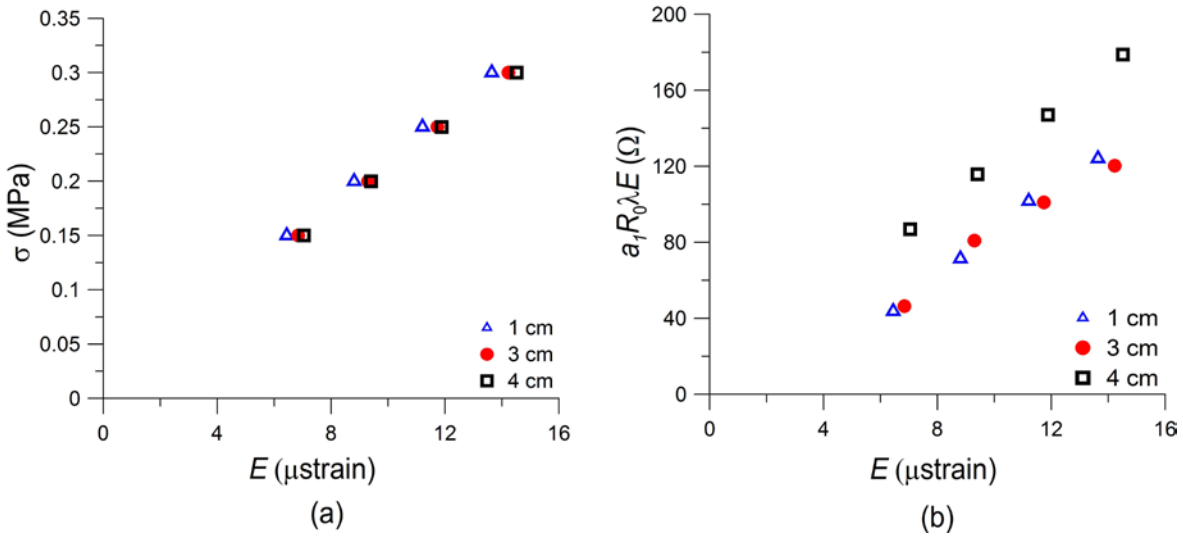

FIGURE 8. Stress-strain behaviour of the sensor (a) and amplitude of first harmonic in Eq. (8) versus the strain amplitude (b).

TABLE 3. Gauge factor.

	Electrodes' distance		
***σ* (MPa)**	**1 cm**	**3 cm**	**4 cm**
0.15	353.9	210.3	258.5
0.20	422.0	254.4	267.3
0.25	473.8	266.1	274.8
0.30	484.8	259.7	263.2

In the considered loading range, the sensor displays a linear stress-strain behaviour, as observed in Figure 8 (a), where σ is the amplitude of the applied oscillatory compressive stress, directly obtained from *N*.

Notably, results of Figure 8 (a) indicate a tangent Young's modulus for the nanocomposite cement paste of approximately 20 GPa. This value is considerably larger than the Young's modulus of plain cement pastes [27,38], and this is likely due to the stiffening effect of the nanoreinforcement and dynamic nature of the test. Results presented in Figure 8 (b) offer further evidence that the presence of superharmonics should not be related to nonlinearities, as we find that the relationship between the amplitude of the first harmonic, Eq. (8), and the amplitude of the axial strain, E, is also approximately linear, independently of the distance between electrodes.

Table 3 displays the gauge factor λ for all the considered experimental conditions. Findings reported therein confirm that λ varies significantly with the distance between the electrodes, while exhibiting smaller variations with the amplitude of the applied axial stress, suggesting that nonlinear phenomena are likely to be secondary.

6. CONCLUSIONS

In this paper, we have assessed a lumped-circuit model to interpret the response of a new nanocomposite cement-based sensor, consisting of a cement paste doped with carbon nanotubes. The lumped-circuit model consists of two resistors and a capacitor, which account for contact resistance, electric polarization, and internal dissipation. Strain sensing is enabled by the change of the electrical properties of the composite as a function of the applied load. Specifically, we propose a linear relationship between the variation of the relative change of the internal electrical resistance and axial strain. The model has been experimentally validated by measuring the step response of unloaded specimens and the steady state response due to harmonic axial compressive loads. Model predictions are in good agreement with experimental findings, offering a solid basis for future work on such sensors, including the development of signal processing tools,

an improved understanding of the dependence of the electrical properties on geometrical and physical factors, and the formulation of design guidelines.

ACKNOWLEDGEMENTS

The authors gratefully acknowledge Prof. J. M. Kenny and the Group of Materials Science of University of Perugia, including Prof. L. Torre, Dr. M. Monti, Dr. M. Natali, and Dr. M. Rallini, for their support in the fabrication and characterization of the sensors. This research was partially supported by Regione Umbria, within POR Umbria ESF 2007-2013, Axis II "Employability" Objective "e" - Axis IV "Human Capital" Objective "l".

REFERENCES

1. Frangopol DM, Kallen MJ, Van Noortwijk JM. Probabilistic models for life-cycle performance of deteriorating structures: review and future directions. *Progr. Str. Eng. Mat.* 2004; 6(4): 197-212

2. U.S. Department of Transportation, Report to Congress - Technical Report, 2008

3. Brownjohn JMW. Structural health monitoring of civil infrastructure. *Philos T. R. Soc. A* 2007; 365(1851): 589-622

4. Mosquera V, Smyth AW, and Betti R. Rapid Evaluation and Damage Assessment of Instrumented Highway Bridges. *Earthquake Eng. Struc.* 2012; 41(4): 755-774

5. Zhou X, Xi L, Lee J. Reliability-centered predictive maintenance scheduling for a continuously monitored system subject to degradation. *Rel. Eng. Syst. Saf.* 2007; 92(4): 530-534

6. Magalhaes F, Cunha E, Caetano E. Vibration based structural health monitoring of an arch bridge: From automated OMA to damage detection. *Mech. Syst. Sig. Proc.* 2012; 28: 212-228

7. Liu M, Frangopol DM, and Kwon K. Fatigue reliability assessment of retrofitted steel bridges integrating monitoring data. *Struct. Saf.* 2010; 32(1): 77-89

8. Han B; Yu X; Kwon E. A self-sensing carbon nanotube/cement for traffic monitoring. *Nanotechnology* 2009; 20: 5pp

9. Yu X; Kwon E. A carbon nanotube/cement composite with piezoresistive properties. *Smart Mater. Struct.* 2009; 18: 5pp

10. Galao O, Baeza FJ, Zornoza E, Garcés P. Strain and damage sensing properties on multifunctional cement composites with CNF admixture. *Cem. Concr. Comp.* 2014; 46: 90-98

11. Chiacchiarelli L, Rallini M, Monti M, Puglia D, Kenny JM, Torre L. The role of irreversible and reversible phenomena in the piezoresistive behavior of graphene epoxy nanocomposites applied to structural health monitoring. *Compos. Sci. Technol.* 2013; 80:73–79

12. Monti M, Natali M, Kenny JM, Torre L. Carbon nanofibers for strain and impact damage sensing in glass fiber reinforced composites based on an unsaturated polyester resin. *Polym. Compos.* 2011; 32(5): 766-775

13. Mondal P, Shah SP, Marks LD. Nanoscale characterization of cementitious materials. *ACI Mat. J.* 2008; 105:174-179.

14. Shah SP, Konsta-Gdoutos MS, Metexa ZS, Mondal P. Nanoscale Modification of Cementitious Materials in *Nanotechnology in Construction 3*, edited by Z. Bittnar et al, Springer, 2009, pp 125-130

15. Cao J, Chung DDL. Electric polarization and depolarization in cement-based materials, studied by apparent electrical resistance measurement. *Cem. Concr. Res.* 2004; 34: 481-485

16. Wen S, Chung DDL. Damage monitoring of cement paste by electrical resistance measurement, *Cem. Concr. Res.* 2000; 30: 1979-1982

17. Azhari F, Banthia N. Cement-based sensors with carbon fibers and carbon nanotubes for piezoresistive sensing. *Cem. Concr. Comp.* 2012; 34: 866-73

18. Han B, Ou J. Embedded piezoresistive cement-based stress/strain sensors. *Sensor Actuat. A - Phys.* 2007; 138: 294-298

19. Wen S, Chung DDL. Partial Replacement of Carbon Fiber by Carbon Black in Multifunctional Cement-Matrix Composites. *Carbon* 2007; 45(3): 505-513

20. Materazzi AL, Ubertini F, D'Alessandro A, Carbon nanotube cement-based transducers for dynamic sensing. *Cem. Conc. Comp.* 2013; 37: 2-11

21. Ubertini F, Laflamme S, Ceylan H, Materazzi AL, Cerni G, Saleem H, D'Alessandro A, Corradini A. Novel Nanocomposite Technologies for Dynamic Monitoring of Structures: a Comparison between Cement-Based Embeddable and Soft Elastomeric Surface Sensors. *Smart Mater. Struct* 2014; 23(4): 12pp

22. Ubertini F, Materazzi AL, D'Alessandro A, Laflamme S. Natural frequencies identification of a reinforced concrete beam using carbon nano tube cement-based sensors. *Eng. Struct.* 2014; 60: 265-275

23. Li GY, Wang PM, Zhao X. Pressure-sensitive properties and microstructure of carbon nanotube reinforced cement composites. *Cem. Concr. Comp.* 2007; 29: 377-382

24. Li H, Xiao H, Ou J. Effect of compressive strain on electrical resistivity of carbon black-filled cement-based composites. *Cem. Concr. Comp.* 2006; 28: 824-828

25. Lourie O, Wagner DE. Buckling and collapse of embedded carbon nanotube. *Phys. rev. Lett.* 1998

26. Han B., Yu X., Ou J. Multifunctional and smart nanotube reinforced cement-based materials. In Nanotechnology in Civil Infrastructure. A Paradigm shift. Gipalakrishnan K., Birgisson B., Taylor P., Attoh-Okine N. Editors, Springer, 2011, 1-48

27. Konsta-Gdoutos MS, Metexa ZS, Shah SP. Highly dispersed carbon nanotube reinforced cement-based materials. *Cem. Concr. Res.* 2010; 40(7): 1052-1059

28. Wen S, Chung DDL. Model of piezoresistivity in carbon fiber cement. *Cem. Concr. Res.* 2006; 36: 1879-1885

29. Li H, Xiao H, Ou J. A study on mechanical and pressure-sensitive properties of cement mortar with nanophase materials. *Cem. Concr. Res.* 2003; 34: 435-438

30. Han BG, Yu Y, Han BZ, JP Ou. Experimental study on use of nickel powder-filled Portland cement-based composite for fabrication of piezoresistive sensors with high sensitivity. *Sensor Actuat. A - Phys.* 2008; 147: 536-543

31. Han B, Guan H, Ou J. Electrode design, measuring method and data acquisition system of carbon fiber cement paste piezoresistive sensors. *Sensor Actuat. A - Phys.* 2007; 135: 360-369

32. Han B, Zhang K, Yu X, Kwon E, Ou J. Electrical characteristics and pressure-sensitive response measurements of carboxyl MWNT/cement composites. *Cem. Concr. Comp.* 2012; 34: 794-800

33. Park KT, Kim SH, Park HS, Lee KW. The determination of bridge displacement using measured acceleration. *Eng Struct* 2005; 27(3): 371-378.

34. Li H, Xiao H, Ou J. Electrical property of cement-based composites filled with carbon black under long-term wet and loading conditions. *Compos Sci. Technol.* 2008; 68(9): 2114-2119.

35. Verhulst F. Linear System Theory, Prentice Hall, 1993, pp356

36. Rugh WJ. Nonlinear Differential Equations and Dynamical Systems, Springer-Verlag, 1990, pp277

37. Bard AJ, Faulkner LR. Electrochemical methods: fundamentals and applications, John Wiley & Sons, 2001, pp 833

38. Abu Al.Rub RK, Ashour AI, Tyson BM. On the aspect ratio effect of multi-walled carbon nanotube reinforcements on the mechanical properties of cementitious nanocomposites. *Constr. Build. Mater.* 2012; 35: 647-655